



Contents lists available at ScienceDirect

## Journal of Sound and Vibration

journal homepage: [www.elsevier.com/locate/jsv](http://www.elsevier.com/locate/jsv)

# Multiple zero-group velocity resonances in elastic layered structures

E.V. Glushkov\*, N.V. Glushkova

Institute for Mathematics, Mechanics and Informatics, Kuban State University Krasnodar, Russia



## ARTICLE INFO

## Article history:

Received 29 June 2020  
 Revised 5 February 2021  
 Accepted 8 February 2021  
 Available online 10 February 2021

## Keywords:

Backward mode  
 ZGV mode  
 Resonant wave excitation  
 Green's matrix based simulation

## ABSTRACT

To date, the phenomenon of zero group velocity (ZGV) Lamb wave in a stress-free elastic plate has been well studied and used in non-destructive material characterization, electroacoustic devices and some other applications. This phenomenon is associated with the backward mode appearing in the range limited by the ZGV and cutoff frequencies. The modal frequency response of the structure, primarily the spectrum of the corresponding guided wave (GW) excited in the plate by a force source, is featured by a sharp peak at the ZGV frequency, allowing its experimental detection. Other peaks appearing at the cutoff frequencies indicate thickness resonances. In a layered half-space of infinite thickness, the backward-mode bend of the dispersion curve turns into a double bend that gives rise to three GWs associated with the same branch (one backward and two forward modes). Moreover, several adjacent branches with double bends, and, thus, several peaks, can appear in a narrow range as the number of layers increases, indicating multiple ZGV resonances. Such dispersion curves with double ZGV points were also found in waveguides of finite thickness with anisotropic or contrast material properties; however, their resonance manifestation is poorly studied. In this article, we consider and discuss several kinds of multi-peak ZGV responses using examples of layered samples of various materials. Along with the expected increase in the number of peaks in multilayer structures with contrast layers, it was noted that some ZGV points may or may not appear in peaks, depending on the type of load.

© 2021 Elsevier Ltd. All rights reserved.

## 1. Introduction

The backward waves are guided waves (GWs) with opposite phase and group velocities, in which the phase moves to the wave source. The history of their study has more than a hundred years, starting with the pioneering work of Lamb in 1904 [1]. The existence of backward Lamb waves in elastic plates has been shown by Tolstoy and Uzdin [2] and experimentally confirmed by Burliy and Kucherov [3].

Backward-wave mode is indicated by a typical bend of the dispersion curve with a negative slope resulting in the negative group velocity of the corresponding guided wave. At the minimum frequency of the backward-wave range, the group velocity becomes zero while the wavenumber remains nonzero; the corresponding wave is referred to as a zero group velocity (ZGV) mode. Besides the opposite phase movement, which detection is a rather challenging task, the backward wave manifests itself by a surface displacement resonance at the ZGV frequency. The maximum backward-wave frequency is the

\* Corresponding author.

E-mail address: [evg@math.kubsu.ru](mailto:evg@math.kubsu.ru) (E.V. Glushkov).

cutoff frequency, at which the real dispersion curve starts. The wavenumber nullifies here together with the group velocity, yielding oscillations independent of spatial coordinates, referred to as a thickness resonance.

Along with stress-free plates, the backward-wave bends of dispersion curves were also found in rigidly supported (bottom-clamped) elastic layers [4]. But for a long time, there were no more examples of isotropic elastic layered waveguides supporting backward modes. In particular, it was believed that backward waves and, thus, ZGV resonances could not occur in a layered half-space of theoretically infinite thickness due to a downward energy outflow into the underlying half-space. Nevertheless, the appearance of backward waves in layered half-spaces has been shown by a gradual softening of the rigid foundation in the bottom-clamped model, i.e., by its gradual transition to a bi-layer half-space [5]. Along the way, it was found that the curve bend, engendering the backward mode, transformed in a double turn that gives rise to three GWs associated with the same branch (one backward and two forward modes; e.g., Fig. 6(b) in Section 4). The negative slope occurs here not from the beginning of the branch, and the backward mode range is limited by two ZGV frequencies instead of the cutoff point as the maximum frequency inherent for a homogeneous guide of finite thickness. Consequently, a double (twin-peak) ZGV resonance should emerge here instead of one conventional ZGV resonance at the minimum frequency and a thickness resonance at the maximum frequency of the range.

In addition to two-layer half-spaces, paper [5] gave examples of double-ZGV dispersion curves in a three-layer half-space with a soft interlayer. And two pairs of ZGV points of adjacent branches turned out to be in a relatively narrow band, which should have led to a multi-peak resonance response on an external load. However, we did not study the frequency response at that time; the paper was focused on the wave energy transfer from the source (surface load) into the structure and its distribution among the excited GW modes and body waves. The energy flow was visualized by energy streamlines. It was shown that in the vicinity of backward-mode and ZGV frequencies, such unusual phenomena as the emergence of energy vortices and backward fluxes occurred. In these processes, ZGV resonances manifested themselves in a sharp redistribution of the source power.

The excitability of ZGV resonances was also out of focus because these phenomena were mostly considered in the context of geophysics, seismic prospecting, civil engineering, and similar applications, assuming vibration of massive objects on an elastic foundation or dynamic contact impact on the surface. A strict solution to the dynamic contact problems reduced to boundary integral equations has shown that the dynamic contact stiffness of the elastic substrate tends to zero at ZGV and cutoff frequencies (e.g., [6,7]). Since the dynamic stiffness enters the formulas for a forced displacement of a massive contacting object together with the inertia terms, its nullification does not affect the amplitude of oscillation. Simultaneously, its resonance increase can occur at completely different frequencies, where these terms cancel each other [6].

Therefore, it was also difficult to excite and detect ZGV resonances by means of ultrasonic transducers in contact with the surface. But with the advent of non-contact laser measurement technology, ZGV resonance became detectable [8–10] that paved the way for the development of laser-based technologies for express evaluating the thickness and material constants of isotropic plates [11,12]. Currently, these technologies are developed for homogeneous plates without the use of multi-peak ZGV resonances.

The promising potential of ZGV resonance methods has revived interest in backward modes, stimulated studies for elastic waveguides of more complex structures, and caused a significant increase in publications in recent years. Most of the research is focused on the analysis of dispersion curves for various waveguides without touching the issues of ZGV resonance excitability. In this way, double-ZGV points (doubly-turned curves) inherent in layered half-spaces [5] were also revealed for elastic waveguides of finite thickness [13–17]; and the occurrence of backward waves in a layered half-space was confirmed [18,19]. The appearance of double-ZGV curves in these guides was due to contrast layering [13,15,16,18] and anisotropy [14,17].

It should also be noted the investigations of the influence of layering [13,20,21] and anisotropy [22,23] on the backward mode and related ZGV effects. A remarkable result of work [22] is a closed-form expression for the Lamb-wave branches at their onset derived for an arbitrary anisotropic plate. It reveals the existence of backward Lamb modes without calculating the dispersion curves in the classical case of single-ZGV bends. Unfortunately, this method cannot indicate a double-ZGV curve that starts as a usual branch.

As for the excitability of ZGV resonances, their study cannot rely only on the analysis of dispersion curves. It requires the use of so-called forced solutions that account for the wave source, allowing estimation of the structural frequency response. Therefore, the number of works in this area is much more modest [15,16,24]. Closest to our work is paper [24], in which the modal excitability in homogeneous and layered elastic and viscoelastic waveguides is investigated using the semi-analytical finite element method (SAFE). It gives an example of a ZGV resonance response of a homogeneous steel plate in the classical  $S_1 - S_2$  single-ZGV point case.

The studies of Ref. [16] are led by the idea to exploit ZGV features to design electroacoustic resonators consisting of a thin piezoelectric  $AlN$  film on a silicon substrate. The curves of phase and group velocities calculated for this structure exhibit both single-ZGV and double-ZGV bends (the latter only for the higher tenth mode). And the admittance with the resonance peaks at ZGV frequencies is nothing but the structural response providing a quantitative estimate of the modal excitability.

The object of investigation in Ref. [15] (fluid-filled pipes) differs from the plane-parallel layered structures with contrast lamina considered in the present paper. Nevertheless, it possesses very similar ZGV features. The dispersion curves of guided (tube) waves generated by a monopole source can also have one or two ZGV points, and the displacement amplitude exhibits peak modal responses at ZGV frequencies.

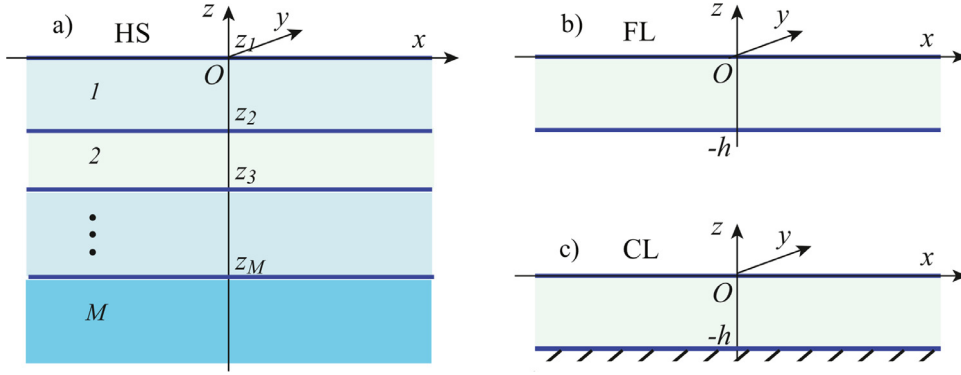


Fig. 1.  $M$ -layered half-space HS (a); free-free layer FL (b); and free-clamped layer CL (c).

The authors of paper [15] also note that the results obtained implies that the ZGV technique has the potential to be applied for in-service inspection of pipelines which are carrying liquid. Similarly, multi-peak ZGV response can be used to detect and estimate a fouling deposition in pipelines [25], including wax deposition in gas and oil pipelines [26]. Since the number and position of resonance peaks in the frequency response are sensitive to changes in elastic properties and thicknesses, another potential application is the ultrasonometric diagnosis of bone osteoporosis [27,28]. Along with the above-mentioned material characterization and electroacoustics, this is a motivation for further ZGV investigation not only of the GW dispersion properties but also their manifestation in multi-peak frequency responses for various layered structures.

To make the presentation more understandable, we tried to give all the necessary theoretical information in the mathematical framework (Section 2) and discuss the characteristic features of ZGV manifestation, first, in a classical homogeneous elastic layer (Section 3). In this section, an example of experimental verification of the mathematical model is also given. The consideration of multilayered structures begins with examples showing the existence of backward modes in a two-layer half-space and differences in ZGV effects compared with the previous case of a free-free or free-clamped layer (Section 4). In Section 5, multiple ZGV resonances in various two- and three-layer structures are considered and discussed with the concluding remarks in Section 6. The frequency response is considered for two kinds of loads: tangential and normal, and it is noted that not all ZGV points may manifest itself in resonance peaks with different loadings.

## 2. Mathematical framework

Consider time-harmonic oscillation  $\mathbf{u}(\mathbf{x}, \omega)e^{-i\omega t}$  of an elastic laminate structure;  $\omega = 2\pi f$ ,  $f$  is frequency. In Cartesian coordinates  $\mathbf{x} = (x, y, z) \equiv (x_1, x_2, x_3)$ , the complex displacement amplitude  $\mathbf{u} = (u, v, w) = (u_1, u_2, u_3)$ . The structure occupies the domain  $D: |x| < \infty, |y| < \infty, -H < z \leq 0$ , which consists of  $M$  sublayers  $D_m: |x| < \infty, |y| < \infty, z_{m+1} \leq z \leq z_m$ ,  $m = 1, 2, \dots, M$ ,  $z_1 = 0, z_{M+1} = -H, D = \cup_{m=1}^M D_m$  (Fig. 1(a)). The thicknesses of the sublayers are  $h_m = z_m - z_{m+1}$ , and the total thickness of the structure is  $H = \sum_{m=1}^M h_m$ . It can be either a finite laminate plate ( $H < \infty$ ) or an infinite multilayered half-space ( $H = \infty$ ).

In the case of anisotropic elastic properties, the components of the complex displacement amplitude  $\mathbf{u}(\mathbf{x}, \omega)$  obey the elastodynamic equations

$$C_{ijkl}u_{i,jk} + \rho\omega^2u_i = 0, \quad i = 1, 2, 3, \quad (1)$$

where stiffness tensor  $C_{ijkl}$  and the density  $\rho$  are piecewise constant functions of the transverse coordinate  $z$ , which keeps constant values within each sublayer  $D_m$ . In the particular case of isotropic sublayers, Eq. (1) is reduced to the Navier-Lamé equation

$$(\lambda + \mu)\nabla\text{div}\mathbf{u} + \mu\Delta\mathbf{u} + \rho\omega^2\mathbf{u} = 0 \quad (2)$$

with two independent elastic moduli (Lamé constants)  $\lambda$  and  $\mu$ . From now on, the time-harmonic factor  $e^{-i\omega t}$  is conventionally omitted.

The sublayers are perfectly bonded with each other, i.e., the displacement vector  $\mathbf{u}$  and the stress vector  $\boldsymbol{\tau} = (\tau_{xz}, \tau_{yz}, \sigma_z)$  are continuous functions of  $z$ . The upper surface  $z = 0$  is stress-free except in a limited area  $\Omega$  with a given surface load  $\mathbf{q}$  simulating a wave source:

$$\boldsymbol{\tau}|_{z=0} = \mathbf{q} \quad (\mathbf{q}(x, y) \equiv \mathbf{0} \text{ for } (x, y) \notin \Omega). \quad (3)$$

In the case of elastic plate ( $H < \infty$ ), the bottom side  $z = -H$  can be either free ( $\boldsymbol{\tau}|_{z=-H} = 0$ ) or clamped ( $\mathbf{u}|_{z=-H} = 0$ ). These two cases are referred to below as the free layer (FL) and the clamped layer (CL) (Fig. 1(b,c)). At infinity ( $r = \sqrt{x^2 + y^2} \rightarrow \infty$  and  $z \rightarrow -\infty$ ), the radiation conditions resulting from the principle of limiting absorption hold [29].

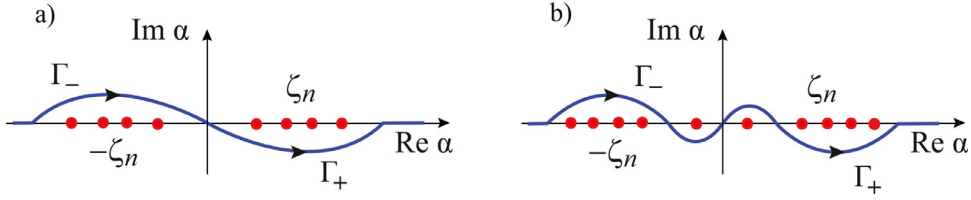


Fig. 2. Semi-infinite contour  $\Gamma_+$  and centrally-spread contour  $\Gamma = \Gamma_- \cup \Gamma_+$  in the regular case (a) and with a backward-mode pole (b).

The guided waves (GWs) under study are eigensolutions  $\mathbf{u}_n$  of Eqs. (1) or (2) that satisfy the homogeneous boundary conditions at the plane-parallel surfaces and interfaces  $z = z_m$ ,  $m = 1, 2, \dots, M + 1$ . Plane GWs propagating along the  $x$ -axis can be written in the form

$$\mathbf{u}_n(\mathbf{x}) = \mathbf{b}_n(z)e^{i\zeta_n x}, \quad n = 1, 2, 3, \dots \quad (4)$$

where the wavenumbers  $\zeta_n$  are spectral points of the boundary value problem (BVP) under consideration, and the amplitude factors  $\mathbf{b}_n$  are the corresponding transverse eigenforms. Being the roots of the characteristic (dispersion) equation

$$\Delta(\zeta, \omega) = 0, \quad (5)$$

they continuously depend on the angular frequency  $\omega$  specifying dispersion curves  $\zeta = \zeta_n(\omega)$  in the plane  $(\omega, \zeta)$ . With real  $\zeta_n$ , GWs (4) propagate with the phase velocities  $c_n = \omega/\zeta_n$ , slownesses  $s_n = \zeta_n/\omega$ , and group velocities  $v_n = d\omega/d\zeta_n$ .

To the present, there have been developed a variety of methods for calculating GW characteristics, including in the case of generally anisotropic laminates (e.g., [30–33]). These methods are sufficient for tracing and analyzing dispersion curves while, with a conventional modal analysis technique, the amplitude eigenvectors  $\mathbf{b}_n$  can only be obtained up to constant factors. However, it is not sufficient for the study of resonance effects, which requires working with unambiguous amplitude-frequency characteristics of source-generated traveling waves. Therefore, for a semi-analytical analysis of forced wave propagation in laminate structures, we traditionally use the Green's matrix based approach [5,34,35] in the form and notations laid down by Vorovich and Babeshko [4].

The unique solution of the BVP considered, i.e., the complex amplitude  $\mathbf{u}$  of the wave field generated in the structure  $D$  by a surface load  $\mathbf{q}$ , is represented as a convolution of the Green's matrix of the structure  $k(\mathbf{x})$  with  $\mathbf{q}$ , or in terms of the inverse Fourier transform of  $\mathbf{U} = K\mathbf{Q}$ , where  $K = \mathcal{F}_{xy}[k]$ ,  $\mathbf{Q} = \mathcal{F}_{xy}[\mathbf{q}]$ , and  $\mathcal{F}_{xy}$  is the operator of the Fourier transform with respect to the horizontal coordinates  $x$  and  $y$  [34]:

$$\begin{aligned} \mathbf{u}(\mathbf{x}, \omega) &= (k * \mathbf{q})(\mathbf{x}) = \int_{\Omega} k(x - \xi, y - \eta, z) \mathbf{q}(\xi, \eta) d\xi d\eta = \\ &= \mathcal{F}_{xy}^{-1}[\mathbf{U}] = \frac{1}{(2\pi)^2} \int_{\Gamma_+} \int_0^{2\pi} K(\alpha, \gamma, z) \mathbf{Q}(\alpha, \gamma) e^{-i\alpha(x \cos \gamma + y \sin \gamma)} d\gamma \alpha d\alpha. \end{aligned} \quad (6)$$

The columns  $\mathbf{k}_j$  of the  $3 \times 3$  Green's matrix  $k = (\mathbf{k}_1; \mathbf{k}_2; \mathbf{k}_3)$  are the displacement vectors corresponding to the point loads  $\tau = \delta(x, y) \mathbf{i}_j$  applied to the surface  $z = 0$  along the coordinate vectors  $\mathbf{i}_j$ ,  $j = 1, 2, 3$ ;  $\delta$  is Dirac's delta-function. The integration path  $\Gamma_+$  goes in the complex plane  $\alpha$  along the real positive semi-axis rounding the real poles of  $K$  elements in accordance with the principle of limiting absorption (Fig. 2). The latter gives a rule for bypassing real positive poles from below almost always, except in the rare case of a backward mode pole that must be bypassed oppositely [4] (Fig. 2(b)).

Applying the residue technique to the path integral gives the source-generated GWs as residues from the poles of matrix  $K$  elements. The contour  $\Gamma_+$  is centrally unfolded on the entire axis, and the resulting path  $\Gamma = \Gamma_- \cup \Gamma_+$  is closed upward. A description of this procedure can be found in Ref. [34]. As a rule, in the absence of backward waves, only positive real poles, which are bypassed from below (Fig. 2(a)), get into the closed contour. They give outgoing GWs with phase and group velocities directed from the source. In the backward mode case, the corresponding pole lies below the path  $\Gamma_+$  and, therefore, outside the closed contour. Thus, it does not contribute to the wavefield representation in terms of GWs. At the same time, its negative counterpart lies above the contour  $\Gamma$  (Fig. 2(b)), getting inside and yielding a backward GW, which propagates from the source with a positive group velocity ( $v_n > 0$ ) but exhibiting a negative phase motion ( $c_n < 0$ ).

For simplicity and clarity, we restrict ourselves to the case of a horizontal or vertical point source  $\mathbf{q} = \delta(x, y) \mathbf{i}_j$ ,  $j = 1$  or 3, and the direction of propagation along the  $x$ -axis, which coincides with a principal material axis if the structure is anisotropic. In such a case,

$$\mathbf{u}(x, y, z) = \sum_{n=1}^{N_r} \mathbf{b}_n(z) e^{ij_n \zeta_n x} / \sqrt{\zeta_n x} [1 + O((\zeta_n x)^{-1})], \quad x \rightarrow \infty. \quad (7)$$

Here  $N_r$  is the number of positive real poles  $\zeta_n$  of the matrix  $K$  elements;  $j_n$  is an indicator of the backward mode: nearly always  $j_n = 1$ , except in the case of backward GW for which  $j_n = -1$ , and the negative counterpart  $-\zeta_n$  contributes into the

modal expansion (7) instead of  $\zeta_n$ , without changing the number of excited traveling waves  $N_r$ ;

$$\mathbf{b}_n(z) = \sqrt{\frac{i}{2\pi}} j_n \zeta_n \text{res} K(-\alpha, 0, z)|_{\alpha=j_n \zeta_n} \mathbf{Q}; \quad \mathbf{Q} = \mathbf{i}_j, \quad j = 1 \text{ or } 3. \tag{8}$$

The terms of expansion (7) are similar to eigensolutions (4). Moreover, the poles  $\zeta_n$  coincide with the roots of dispersion equation (5), since its left part  $\Delta$  is nothing but a common denominator of matrix  $K$  elements; and the functions  $\mathbf{b}_n(z)$  specified in Eq. (8) are of the same shapes as the eigenforms  $\mathbf{b}_n(z)$  in Eq. (4). But unlike the latter, they are uniquely determined in Eq. (8) via the Fourier symbols of the structure's Green's matrix  $k$  and the given load  $\mathbf{q}$ .

With the selected tangential or normal point load  $\mathbf{q}$ , the amplitude vector  $\mathbf{b}_n$  of each mode coincides, up to the factor  $\sqrt{i/2\pi} j_n \zeta_n$ , with the first or third column of the residue matrix  $\text{res} K$ . Therefore, in order to estimate the contribution of each mode into the structure's response, it suffices to consider the frequency dependences of its elements:  $a_{n,ij}(f) = |\text{res} K_{ij}|$  at  $z = 0$ , while the sum of such modal responses estimates the maximum of the total response:

$$a_{ij}(f) = \sum_{n=1}^{N_r} a_{n,ij}(f). \tag{9}$$

In the discussion below, these functions are referred to as the amplitudes of frequency spectra of the corresponding modal components, neglecting the insignificant factors  $\sqrt{i/2\pi} j_n \zeta_n$ . The vertical point load simulates a laser beam action on the surface while the third displacement vector component describes the out-of-plane surface response measured by a laser Doppler vibrometer. Therefore, the functions  $a_{n,33}(f)$  are of prime concern for the surface acoustic wave (SAW) laser generation and measurement technique. The tangential point load is used in the pin-force models of Lamb wave excitation and detection by piezoelectric active wafer sensors [36], for which the functions  $a_{n,11}(f)$  are of interest.

### 3. Backward modes and ZGV resonance in an elastic layer

To analyze the manifestation of backward modes and ZGV resonance effects, we start with a homogeneous layer. Fig. 3 gives examples of dispersion curves for two kinds of such waveguides: a stress-free layer (FL) and a bottom-clamped layer

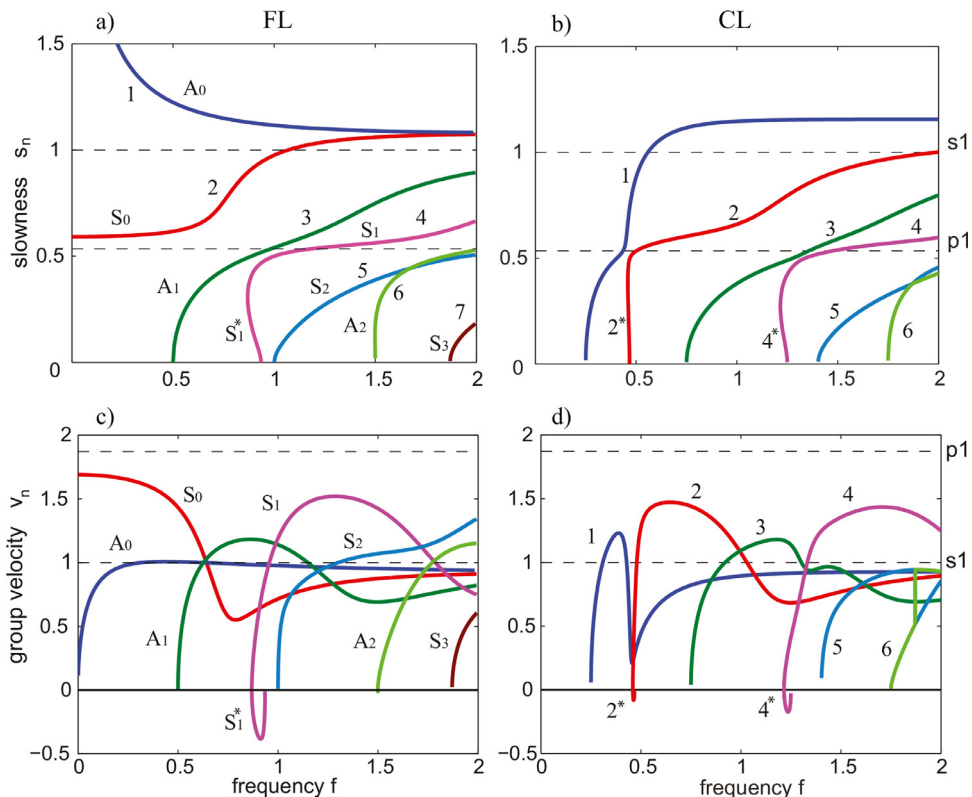


**Fig. 3.** Dimensionless dispersion curves for a free (FL) (a,c) and clamped (CL) (b,d) layers; top (a,b) for slownesses, bottom (c,d) for group velocities as functions of frequency. Horizontal dashed lines are for the frequency-independent body wave slownesses (top) or velocities (bottom) marked with 'p1' and 's1' for P and S body waves.

**Table 1**  
Dimensionless parameters of sublayers.

material No	$c_p$	$c_s$	$\rho$	$h$	$E$	$\nu$
I	1.87	1.	1.	1.	2.6	0.3
II	40.	20.	1.	1.	1067.	0.333
III	10.	1.	1.	1.	2.990	0.495
IV	20.	10.	1.3	$\infty$	346.7	0.333
V	5.221	2.887	19.254	0.05	410.8	0.280
VI	3.	1.	1.	1.	2.875	0.438

(CL). It shows the slownesses  $s_n(f)$  and group velocities  $v_n(f)$  as functions of dimensionless frequency  $f$ . For generality and comparability, hereinafter (unless otherwise indicated), the numerical results are presented in dimensionless form. As the base units  $l_0$ ,  $c_0$ , and  $\rho_0$ , we chose the thickness  $h$ ,  $S$ -wave velocity  $c_s$ , and density  $\rho$  of the layer:  $l_0 = h$ ,  $c_0 = c_s$ , and  $\rho_0 = \rho$ ; the unit of frequency is  $f_0 = c_0/l_0$ , the unit of elastic moduli is  $E_0 = \rho_0 c_0^2$ . The curves of Fig. 3 are calculated for the input parameters of material I given in the first line of Table 1. For convenience, along with the four independent parameters  $c_p$ ,  $c_s$ ,  $\rho$  and  $h$ , dimensionless Young's modulus  $E$  and Poisson's ratio  $\nu$  are also shown in the table.

Depicting dispersion curves in the frequency-slowness plane is more convenient. In contrast with the wavenumber curves  $\zeta_n(f)$  that goes up to infinity or phase velocity curves  $c_n(f)$  that come down from infinity, the slowness magnitudes vary in a limited range specified by the frequency-independent bulk-wave and Rayleigh wave slownesses (except the  $A_0$  mode curve in a free layer).

Backward traveling waves arise in those frequency ranges where the curves have a specific bend with a negative tangent slope. For example, in the FL sample (Fig. 3(a)), the backward modes appear in the fourth ( $S_1$ ) branch in the range  $0.869 < f < 0.935$  and in the sixth ( $A_2$ ) branch in the very narrow band  $1.4987 < f < 1.5000$ . In these ranges, each bend yields two wavenumbers for the forward and backward guided waves associated with the same  $n$ th dispersion curve:  $\zeta_n = \omega s_n$  and  $\zeta_n^* = \omega s_n^*$ . At the left end (the minimum frequency) of the range, these two wavenumbers merge in a double root of the dispersion equation, and the tangent to the curve at this point ( $f_{ZGV}$ ,  $\zeta_{n,ZGV}$ ) becomes vertical. Accordingly, the group velocity  $v_n = d\omega/d\zeta_n$  of the associated traveling wave  $\mathbf{b}_n(z)e^{i\zeta_n z}$  is equal to zero, and such a normal mode is referred to as a ZGV mode [8]. The wavenumber of the ZGV mode is nonzero:  $\zeta_{n,ZGV} \neq 0$ , while at the right end of the range  $\zeta_n = 0$ . Here the range is limited by the cutoff frequency  $f_c$  (the onset point of the real branch of the dispersion curve), at which the group velocity  $v_n$  is also equal to zero. In the range  $f_{ZGV} < f < f_c$ , the group velocity is negative, and its curve exhibits a typical open half-loop in the low half-plane of the  $(f, v_n)$  plane (Fig. 3(c,d)).

The double root  $\zeta_{n,ZGV}$  is a double pole of  $K_{ij}$ , at which the residues  $\text{res}K_{ij}$  can increase to infinity, manifesting itself in ZGV resonance peaks in the frequency spectra  $a_{ij}(f)$ . Expanding the numerator and denominator of the matrix  $K$  elements in a Taylor series in the vicinity of double roots ( $f_{ZGV}$ ,  $\zeta_{ZGV}$ ) of equation (5), including the cutoff points ( $f_c$ , 0), one can show that these frequencies are the points of weak (root) singularity of the frequency spectra:  $a_{ij}(f) \sim O(|f - f_{ZGV}|^{-0.5})$  as  $f \rightarrow f_{ZGV}$ , and  $a_{ij}(f) \sim O(|f - f_c|^{-0.5})$  as  $f \rightarrow f_c$ . The latter indicates a thickness resonance that occurs when an even (FL) or odd (CL) number of  $P$  or  $S$  body quarter waves fits into the layer thickness. The resonance response of the FL and CL plates is illustrated by the  $a_{11}$  and  $a_{33}$  plots of Fig. 4.

As an example of experimental verification of the computer model, we imposed the curves  $a_{n,33}$  for the regular and backward modes  $S_1$  and  $S_1^*$  (Fig. 5, dashed lines) on the copied from Ref. [23] plot of the laser-generated and optically measured surface displacement of a free [001]-cut silicon plate (solid line). The figure provides an expanded view of the  $S_1$  ZGV resonance and thickness resonance peaks similar to the resonance peaks at the  $S_1$   $f_{ZGV} = 0.869$  and  $f_c = 0.935$  in Fig. 4(c). Unlike the FL example, this plate is anisotropic (cubic symmetry) specified by the three independent elastic constants  $C_{11} = 165.6$ ,  $C_{12} = 63.9$  and  $C_{44} = 79.5$  (GPa), density  $\rho = 2329$  kg/m<sup>3</sup>, and thickness  $h = 0.525$  mm; the frequency is in megahertz. Due to anisotropy, the value of  $f_{ZGV}$  depends on the propagation direction.

It varies from 7.71 MHz for the azimuth angle  $\varphi = 0$  to 7.75 MHz for  $\varphi = \pi/4$ . At the same time, the cutoff frequency  $f_c = 8.03$  MHz is directionally independent. Since most of the source energy is in the GWs propagating along the principal material axes, and the surface displacement was measured at the same point that the laser beam acted on, both of these frequencies manifest themselves as ZGV resonance peaks in the experimental curve of Fig. 5 [23]. Accordingly, the superimposed curves  $a_{n,33}$  were also calculated for these two propagation directions (color online: red dashed lines for  $\varphi = 0$  and blue ones for  $\varphi = \pi/4$ ). One can see a good agreement between the calculated and measured resonance responses.

#### 4. Layered half-space: existence of backward modes and ZGV frequencies

The split of the ZGV mode resonance into two resonance peaks in Fig. 5 is due to the material anisotropy. Each of the peaks is associated with a single ZGV point on the corresponding dispersion curve. Nevertheless, more than one ZGV point can also be on the same dispersion curve with a specific double bend. To illustrate this fact, we begin with an example confirming the possibility of backward waves in a layered half-space. For a long time, it was believed that traveling backward GWs could not be formed in such structures due to a downward energy outflow into the underlying half-space. On the

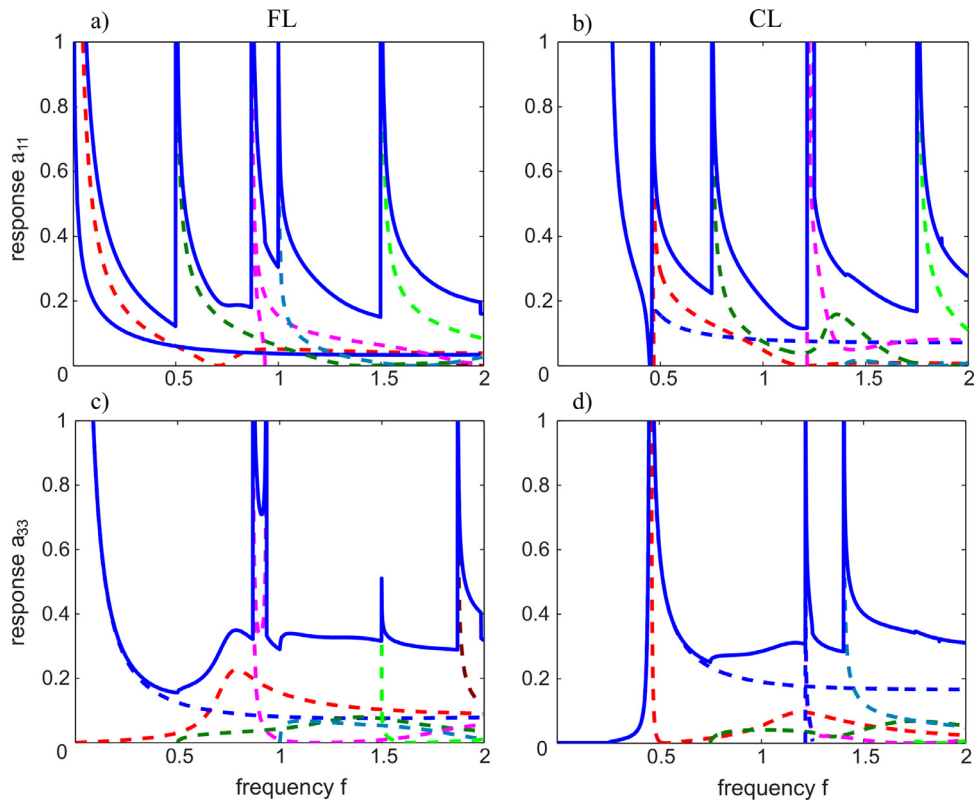


**Fig. 4.** Amplitudes of frequency spectra of the responses  $a_{11}$  and  $a_{33}$  of each mode (dashed lines) and their total sum (solid lines) for the FL (left) and CL (right) plate samples with the GW dispersion properties shown in Fig. 3.

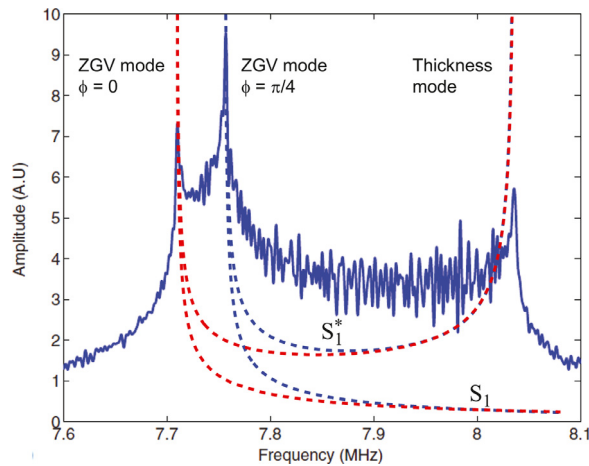


**Fig. 5.** Theory-to-experiment comparison: backward mode range frequency spectrum of laser-generated and optically measured surface displacement of a free silicon plate (solid line, [23]) and the amplitude curves  $a_{n,33}$  for the forward and backward modes  $S_1$  and  $S_1^*$  (dashed lines) calculated for two principal azimuth directions  $\varphi$ .

other hand, they exist in a bottom-clamped (CL) layer. And with a gradual transition from a rigid base to a soft base, e.g., by increasing the ratio  $\varepsilon = c_{p,1}/c_{p,2}$ , the bend of the dispersion curve with a negative tangent should remain in a non-zero interval  $0 < \varepsilon < \varepsilon^*$  ( $c_{p,m}$  is the  $P$ -wave velocity in the  $m$ th sublayer, Fig. 1(a)). Inspired by this idea, we calculated examples of such a gradual transition, confirming the possibility of backward wave propagation in a two-layer half-space [5]. Some other examples of backward-wave modes arising in more complex multilayered half-spaces were also obtained at that time.

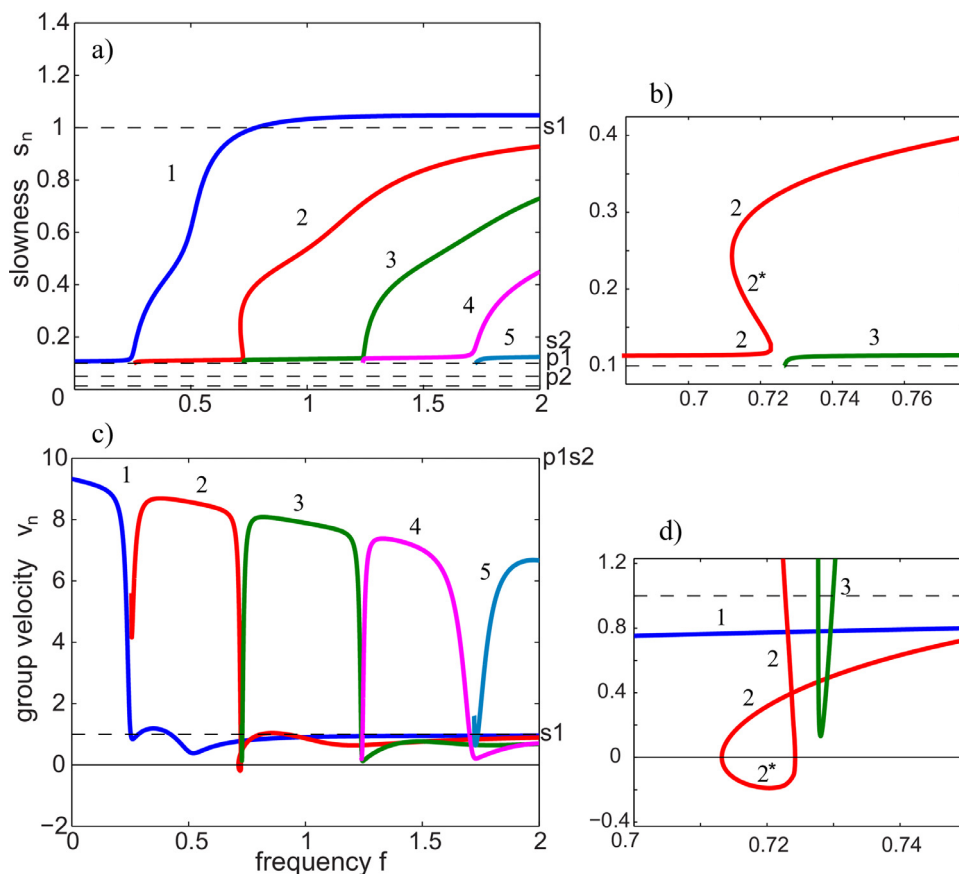


**Fig. 6.** Two-layer elastic half-space HS2-III/IV: left, (a,c), slowness and group velocity; right, (b,d), enlarged backward mode parts.

**Fig. 6** illustrates a typical backward mode appearance in a two-layer elastic half-space with a softer upper layer. The dimensionless properties of its upper layer and base are shown in rows III and IV of [Table 1](#) (denote this structure as HS2-III/IV). Same as in the examples of [Ref. \[5\]](#), this model came from geophysics and vibroseismic prospecting in a marshland. Its upper layer is featured by a relatively low  $S$ -wave velocity:  $\gamma = c_{s,1}/c_{p,1} = 0.1$ , and, consequently, by close to 0.5 Poisson's ratio:  $\nu_1 = 0.495$ , which is typical for liquid-filled soils. The base is a hard ground with  $\nu_2 = 1/3$ , and the contrast of  $P$ -wave velocities  $\varepsilon = c_{p,1}/c_{p,2} = 1/2$ . Layered structures with similar non-dimensional properties can also be found in other areas, for example, plastic and rubber-like coatings or nano-wired polymer composite films [\[37\]](#).

The slowness curves in [Fig. 6\(a\)](#) look similar to those in the CL case ([Fig. 3\(b\)](#)) but, unlike the latter, they do not start from zero values, but exit from the horizontal line of  $S$ -wave slowness in the lower half-space (dashed line 's2' in the case). Formally, in the CL case, the curves also start from the value of  $S$ -wave slowness in the lower rigid substrate, which is equal to zero, and, therefore, the line 's2' coincides with the frequency axis. Before the onset points, the curves are complex branches lying either on the physical or on the unphysical Riemann sheet of the complex  $s$ -plane (the value 's2' is the branch point). Another characteristic feature is that after the exit point, the curves go along the line 's2' for a long while and then sharply turn up near the cut-off frequencies of the corresponding CL guide. Each subsequent GW curve starts close to such an upward turn of the preceding curve. The initial almost horizontal sections of the dispersion curves give traveling waves propagating with high phase and group velocities, induced by the high-speed body waves of the lower half-space. Sharp upward turns indicate a sharp decrease in the GW velocities tending in the limit to the Rayleigh wave velocity, which is relatively small for the soft material of the upper layer. On the group velocity plot ([Fig. 6\(c\)](#)), it looks like narrow splits to almost zero (or lower for the backward modes).

An expanded view of the backward mode curve in [Fig. 6\(b\)](#) shows that the bend inherent in the elastic layer ([Fig. 3\(a,b\)](#)) transforms into a double bend providing two ZGV frequencies:  $f_{ZGV1} = 0.713$  and  $f_{ZGV2} = 0.724$ . The latter is the right limit of the backward mode range instead of the cut-off frequency  $f_c$  in FL and CL samples. Accordingly, the group velocity curve draws a closed loop ([Fig. 6\(d\)](#)) instead of open half-loops in [Fig. 3\(c,d\)](#). Now three GWs correspond to the same curve in the range  $f_{ZGV1} < f < f_{ZGV2}$ : two forward waves and one backward wave. In the enlarged portions shown in [Fig. 6\(b,d\)](#), the corresponding parts of curve 2 are indicated as 2, 2\*, and again 2. As a result, the structure of the resonance peaks also changes.

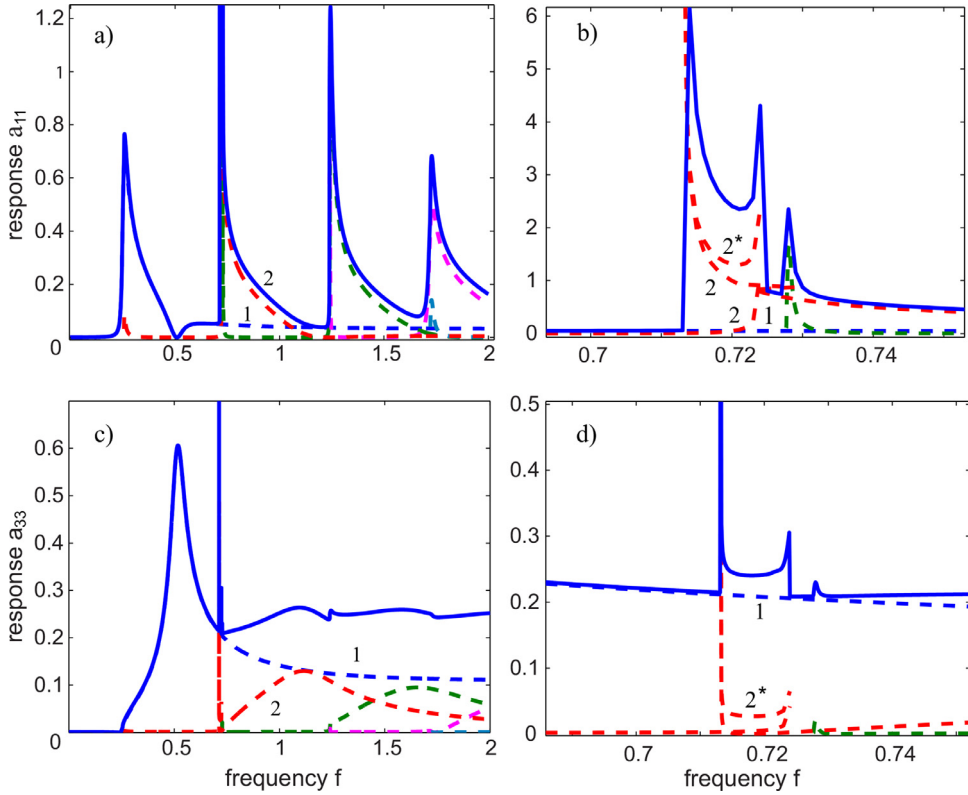


Fig. 7. Modal responses  $a_{11}$  (top) and  $a_{33}$  (bottom) in half-space HS2-III/IV; right subplots provide an enlarged view of ZGV resonance peaks.

## 5. Multiple ZGV resonances

### 5.1. Two-layer half-space

The pattern of resonance peaks of the  $a_{11}$  response of the HS2-III/IV half-space (Fig. 7(a)) is similar to that in the CL case (Fig. 4(b)). The peaks arise at ZGV frequencies and the frequencies of thickness resonance near the upward turns of the preceding curves. The enlarged part of the backward mode range (Fig. 7(b)) shows two peaks at both ends of the backward mode range and a thickness mode peak at the next onset frequency to the right of it. As in the case of a homogeneous layer (e.g., the amplitude of  $S_1^*$  mode in Fig. 5), the amplitude of backward mode  $2^*$  tends to infinity at both ends of the range. But unlike it, there are two forward modes 2 with a singularity either at the left ZGV frequency  $f_{ZGV1}$  or the right frequency  $f_{ZGV2}$ . Note that the curve of the total response (solid line) is without a beating as in Fig. 5 because in Eq. (9), it is introduced not as a sum of complex values but as a sum of their absolute values.

As for the vertical response  $a_{33}$  (Fig. 7(c,d)), the thickness resonances do not appear quite noticeably in this structure, and the ZGV resonance is not as strong as with a tangential load. The contribution of backward mode  $2^*$  and modes 2 to the total response is much less here than that of regular mode 1.

### 5.2. Bottom-clamped layer with a hard coating

A dispersion curve with a typical double bend giving a pair of ZGV points can appear not only in a layered half-space but also in a layered guide of finite thickness. For example, the first curve in Fig. 6(a) from Ref. [13], calculated for in a bottom-clamped (CL) bi-layer structure (thin tungsten layer on a thick bottom-clamped soft layer), has such a bend. To find out how the double-ZGV resonance manifests itself in such a structure, in Figs. 8 and 9, we display the dispersion curves and modal responses in the same format as in the preceding figures. The dimensionless input parameters of this guide are specified in rows V and VI of Table 1 (denote it as CL2-V/VI). The characteristic feature of GW propagation in this structure is that ZGV modes occur in the neighbor curves 1 and 2 at neighbor frequencies  $f_{ZGV1} = 0.300$ ,  $f_{ZGV2} = 0.335$ , and  $f_{ZGV3} = 0.405$  (Fig. 8(a,b)); curve 1 has a double bend, and curve 2 has a conventional single bend. Respectively, the group velocity curve of mode 1 exhibits a full closed loop as in the case HS2-III/IV, while the second curve shows a semi-loop as in the FL or CL guide (Fig. 8(d)).

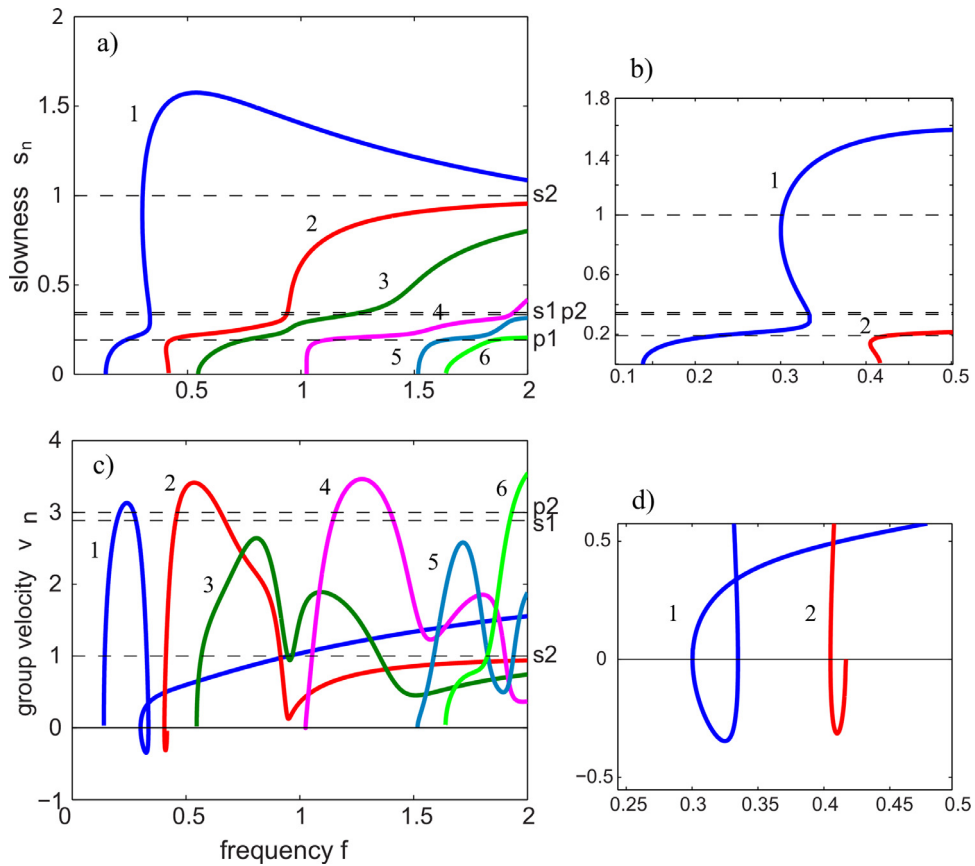


Fig. 8. Bi-layer bottom-clamped guide CL2-V/VI: left, (a,c), slowness and group velocity; right, (b,d), enlarged backward mode parts.

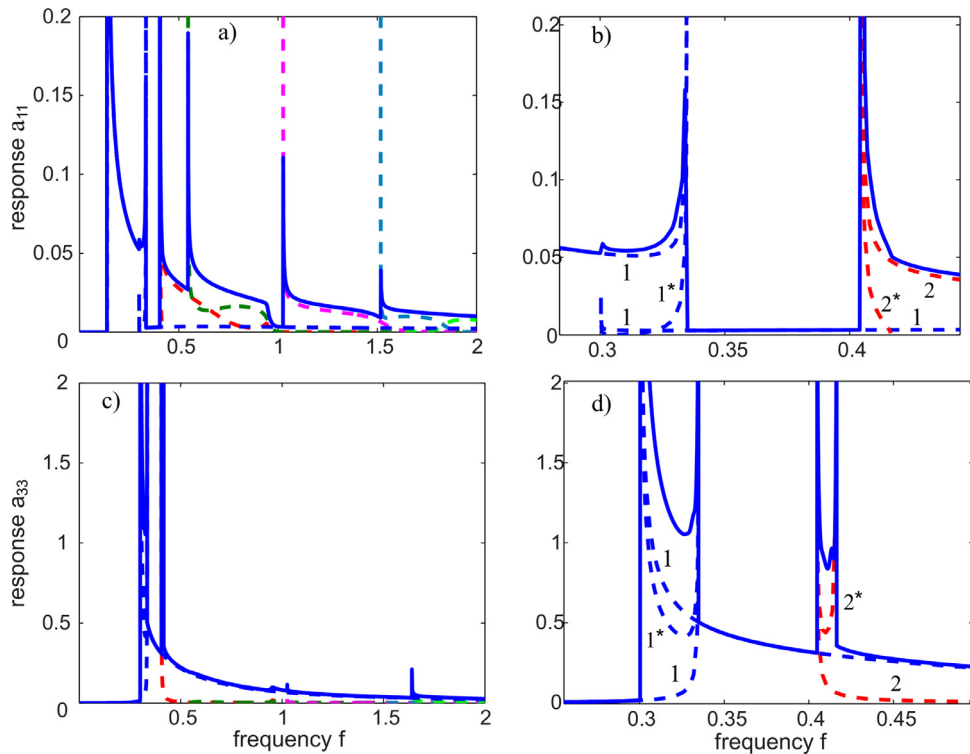
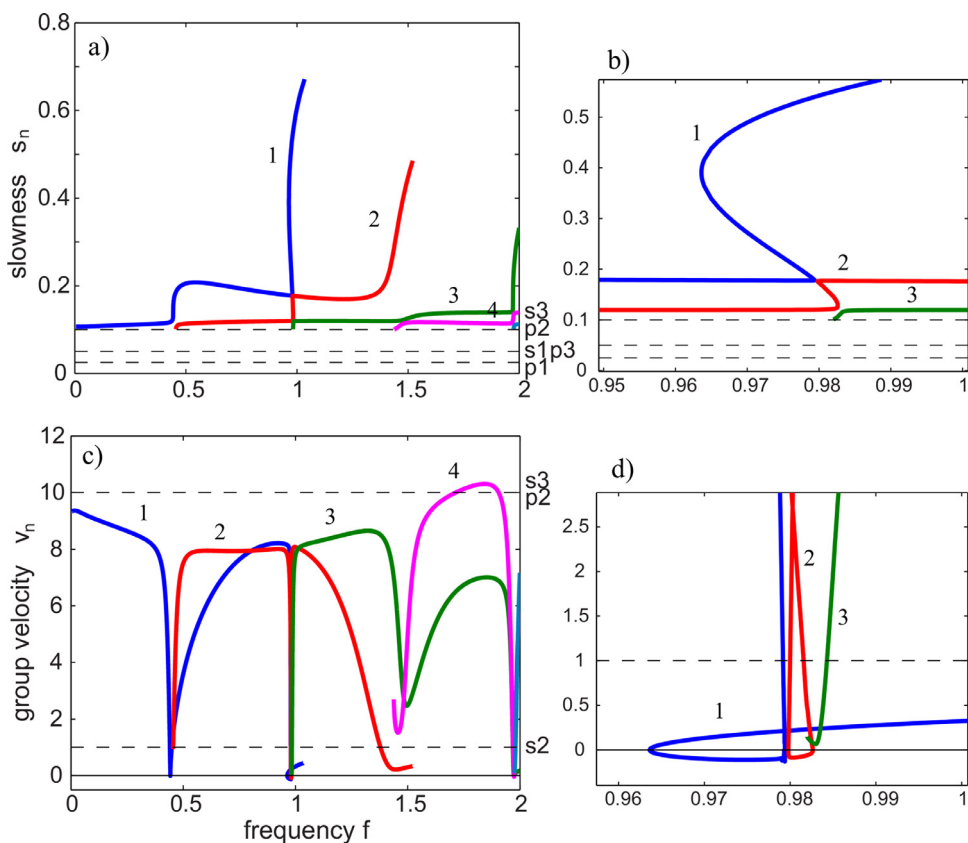


Fig. 9. Modal responses  $a_{11}$  (top) and  $a_{33}$  (bottom) in two-layer guide CL2-V/VI; right subplots give an enlarged view of ZGV resonance peaks.



**Fig. 10.** Same as in Fig. 8 but for the three-layer half-space HS3-II/III/IV: left, (a,c), slowness and group velocities; right, (b,d), enlarged backward mode parts.

Since the hard coating is relatively thin, the general view of the resonance responses shown in Fig. 9(a,c) is similar to the pattern obtained in the CL case (Fig. 4(b,d)). However, an enlarged view of the  $a_{33}$  resonance peaks (Fig. 9(d)) shows that they arise at each ZGV frequency plus a thickness resonance peak at  $f_c = 0.416$ ; a total of four peaks in a narrow frequency band. This is more than in the previous reference cases, namely, than two peaks in the CL case or three peaks in the case of two-layer sample HS2-III/IV (Fig. 7(b,d)). Four peaks appear here because the amplitude of each of the backward modes  $1^*$  and  $2^*$  infinitely increases at both ends of their ranges. However, this is not a general rule but only a potential possibility of a resonance response at each ZGV frequency. Thus, in the response  $a_{11}$ , resonant peaks are observed only at two internal neighboring frequencies:  $f_{ZGV2}$  and  $f_{ZGV3}$  (Fig. 9(b)), while at the leftmost frequency  $f_{ZGV1}$ , the peak is barely visible, and the amplitude of mode  $2^*$  decreases to zero at the right end of its range. That is, this component exhibits a two-peak resonance response instead of possible four-peak resonance.

### 5.3. Three-layer half-space

The following example is for a three-layer half-space with a soft interlayer (Figs. 10 and 11). Its properties are specified by rows II, III, and IV of Table 1, so we denote it HS3-II/III/IV. A similar structure was also considered in Ref. [5] as a model of a winter marshland (the top layer is for frozen liquid-saturated soil or ice). It is obtained from the two-layer model HS2-III/IV by adding a hard coating. This model can also be considered as a transition from the two-layer model CL2-V/VI, in which the rigid base is slightly softened, and the upper hard coating is made relatively thicker. The bi-layer CL2-V/VI also has a soft interlayer sandwiched between two hard solids and forms an inner channel. Therefore, the three-layer structure retains, to some extent, the waveguide properties of both those two-layer waveguides.

At first glance, the dispersion curves in Fig. 10(a) look rather unusual, ending abruptly on the rise. In fact, the curves continue, but as complex branches of pseudo-GWs (evanescent modes). Physically, the pole's shift from the real axis to the complex plane means that the corresponding traveling wave transforms into a leaky guided wave. It propagates in the top hard layer with energy outflow into the underlying soft interlayer and then into the lower half-space. Such an effect is inherent in layered half-spaces with hard coatings. We consider only traveling waves associated with real branches; therefore, we do not plot complex parts of the curves in this figure.

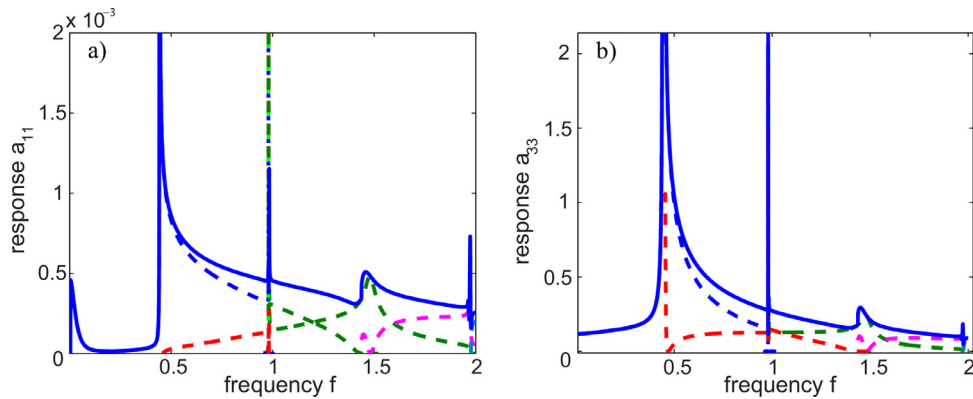


Fig. 11. Modal responses  $a_{11}$  (left) and  $a_{33}$  (right) of the three-layer half-space HS3-II/III/IV.

As for the ZGV modes, curves 1 and 2 have two adjacent double bends (Fig. 10(b)), which yield four ZGV frequencies in a narrow band:  $f_{ZGV} = 0.9636, 0.9794, 0.9798,$  and  $0.9826$ . In addition, the onset frequency of the third mode,  $f_c = 0.9820$ , also lies in this interval  $0.9636 < f < 0.9826$ . Accordingly, the group velocity curves form two closed loops with negative lower parts; and the minimum of the third curve almost reaches zero (Fig. 10(d)). In the plots of modal responses (Fig. 11), this range manifests itself as a high-quality resonance mode, the peak of which is much narrower than a strong thickness resonance peak at  $f_c = 0.454$ . As it follows from the above, the structure could exhibit a five-peak resonance response in this range. However, as in some previous cases (e.g., Fig. 9(b)), not all ZGV frequencies give distinguishable resonance peaks. An enlarged view shows that strong resonances occur only at two adjacent ZGV frequencies:  $f_{ZGV2} = 0.9794$  and  $f_{ZGV3} = 0.9798$ , which differ only in the fourth digit, and there is a weaker peak at  $f_c = 0.9820$ . The two remaining points  $f_{ZGV1}$  and  $f_{ZGV4}$ , which are the external boundaries of these adjacent backward mode ranges, do not work in this case. That is why the corresponding resonance bursts in Fig. 11 look so narrow.

## 6. Concluding remarks

1. The frequency response of layered elastic waveguides to a surface point load is studied on the basis of exact integral representations and explicit guided wave asymptotics with a focus on ZGV resonance manifestation. Starting with ZGV and thickness resonances in a homogeneous elastic layer, which are already well known and used for material characterization, it is shown how the pattern of ZGV resonance peaks changes with the increasing complexity of the waveguide structure (clamped bottom, soft film, hard coating, layered half-space, soft interlayer).
2. In an elastic half-space of infinite thickness, the backward-mode bend of the dispersion curve turns into a double bend. As the number of layers increases, several adjacent branches with double ZGV points may appear in a narrow range, giving rise to a multi-peak resonance response. It is noteworthy that some ZGV points may or may not appear in peaks, depending on the type of load.
3. In addition to material characterization, multiple ZGV resonance effects have a promising potential for developing microelectromechanical systems (MEMS) and nano-composites, bone osteoporosis ultrasound diagnostics, and in-service pipeline inspection, including estimate a fouling deposition.

## Declaration of Competing Interest

The authors declare that they have no known competing financial interests or personal relationships that could have appeared to influence the work reported in this paper.

## CRediT authorship contribution statement

**E.V. Glushkov:** Conceptualization, Funding acquisition, Methodology, Software, Visualization, Investigation, Data curation, Writing - original draft. **N.V. Glushkova:** Conceptualization, Supervision, Methodology, Validation, Visualization, Investigation, Writing - review & editing.

## Acknowledgement

The work is supported by the [Russian Science Foundation](#) (Project No. 17-11-01191).

## Supplementary material

Supplementary material associated with this article can be found, in the online version, at doi:[10.1016/j.jsv.2021.116023](https://doi.org/10.1016/j.jsv.2021.116023).

## References

- [1] H. Lamb, On group velocity, *Proc. L. Math. Soc. Ser. 2* 849 (1) (1904) 473–479.
- [2] I. Tolstoy, E. Usdin, Wave propagation in elastic plates: low and high mode dispersion, *J. Acoust. Soc. Am.* 29 (1957) 37–42.
- [3] P.V. Burliy, I.Y. Kucherov, Backward elastic waves in plates, *Pis'ma Zh. Eksp. Teor. Fiz.* 26 (9) (1977) 644–647. In Russian
- [4] I.I. Vorovich, V.A. Babeshko, Dynamic mixed problems of elasticity for non-classical domains, Nauka, Moscow, 1979. In Russian
- [5] V. A. Babeshko, E. V. Glushkov, N. V. Glushkova, Energy vortices and backward fluxes in elastic waveguides, *Wave Motion* 16 (1992) 183–192.
- [6] V.A. Babeshko, E.V. Glushkov, Z.F. Zinchenko, Dynamics of inhomogeneous linearly elastic media, Nauka, Moscow, 1989. In Russian
- [7] E.V. Glushkov, N. V. Glushkova, Determination of the dynamic contact stiffness of an elastic layer, *PMM U.S.S.R.* 54 (3) (1990) 393–397.
- [8] C. Prada, O. Balogun, T.W. Murray, Laser-based ultrasonic generation and detection of zero-group velocity lamb waves in thin plates, *Appl. Phys. Lett.* 87 (2005) 194109.
- [9] O. Balogun, T.W. Murray, C. Prada, Simulation and measurement of the optical excitation of the S1 zero group velocity lamb wave resonance in plates, *J. Appl. Phys.* 102 (2007) 064914.
- [10] C. Grünsteidl, I.A. Veres, T.W. Murray, Experimental and numerical study of the excitability of zero group velocity lamb waves by laser-ultrasound, *J. Acoust. Soc. Am.* 138 (1) (2015) 242–249.
- [11] C. Prada, D. Clorennec, D. Royer, Local vibration of an elastic plate and zero group velocity lamb modes, *J. Acoust. Soc. Am.* 124 (2008) 203–212.
- [12] C. Grünsteidl, T.W. Murray, T. Berer, I.A. Veres, Inverse characterization of plates using zero group velocity lamb modes, *Ultrasonics* 65 (2016) 1–4.
- [13] A.A. Maznev, A.G. Every, Existence of backward propagating acoustic waves in supported layers, *Wave Motion* 48 (2011) 401–407.
- [14] T. Hussain, F. Ahmad, Lamb modes with multiple zero-group velocity points in an orthotropic plate, *J. Acoust. Soc. Am.* 132 (2) (2012) 641–645.
- [15] H. Cui, W. Lin, H. Zhang, X. Wang, J. Trevelyan, Backward waves with double zero-group-velocity points in a liquid-filled pipe, *J. Acoust. Soc. Am.* 139 (3) (2016) 1179–1194.
- [16] C. Caliendo, M. Hamidullah, Zero-group-velocity acoustic waveguides for high-frequency resonators, *J. Phys. D* 50 (47) (2017) 474002.
- [17] S. Karous, S. Dahmen, M.S. Bouhdima, S. Mohamed, M.B. Amor, C. Glorieux, Multiple zero group velocity lamb modes in an anisotropic plate: propagation along different crystallographic axes, *Can. J. Phys.* 97 (10) (2019) 1064–1074.
- [18] P.G. Malischewsky, T. Forbriger, C. Lomnitz, Unusual, equivocal Rayleigh-dispersion curves for simple models taking into account the special propagation conditions in the valley of mexico city (CDMX) preliminary results, *Geofs. Intl.* 56-1 (2017) 7–12.
- [19] P.G. Malischewsky, T. Forbriger, May rayleigh waves propagate with group- and phase-velocities of opposite sign in the valley of mexico city? *Geofs. Intl.* 59 (2) (2020) 101–104.
- [20] E. Kausel, On the number and location of zero-group-velocity modes, *J. Acoust. Soc. Am.* 131 (5) (2012) 3601–3610.
- [21] S. Mezil, F. Bruno, S. Raetz, J. Laurent, D. Royer, C. Prada, Investigation of interfacial stiffnesses of a tri-layer using zero-group velocity lamb modes, *J. Acoust. Soc. Am.* 138 (2015) 3202–3209.
- [22] A.L. Shuvalov, O. Poncelet, On the backward lamb waves near thickness resonances in anisotropic plates, *Int. J. Solids Struct.* 45 (2008) 3430–3448.
- [23] C. Prada, D. Clorennec, T.W. Murray, D. Royer, Influence of the anisotropy on zero-group velocity lamb modes, *J. Acoust. Soc. Am.* 126 (2009) 620–625.
- [24] F. Treysse, L. Laguerre, Numerical and analytical calculation of modal excitability for elastic wave generation in lossy waveguides, *J. Acoust. Soc. Am.* 133 (6) (2013) 3827–3837.
- [25] H. Lais, P.S. Lowe, T.-H. Gan, L.C. Wrobel, J. Kanfoud, Characterization of the use of low frequency ultrasonic guided waves to detect fouling deposition in pipelines, *Sensors* 18 (2018) 2122.
- [26] H. Liu, Y. Lu, J. Zhang, A comprehensive investigation of the viscoelasticity and time-dependent yielding transition of waxy crude oils, *J. Rheol.* 62 (2018) 527.
- [27] A. Tatarinov, V. Egorov, N. Sarvazyan, A. Sarvazyan, Multi-frequency axial transmission bone ultrasonometer, *Ultrasonics* 54 (2014) 1162–1169.
- [28] J. Schneider, G. Iori, D. Ramiandrisoa, M. Hammami, M. Grsel, C. Chappard, R. Barkmann, P. Laugier, Q. Grimal, J.R. Minonzo, K. Raum, Ex vivo cortical porosity and thickness predictions at the tibia using full-spectrum ultrasonic guided-wave analysis, *Arch. Osteoporos* 14 (2019) 21.
- [29] A.V. Sveshnikov, The limit absorption principle for a wave guide, *Dokl. Akad. Nauk SSSR* 80 (3) (1951) 345–347. (in Russian)
- [30] A.H. Nayfeh, The general problem of elastic wave propagation in multilayered anisotropic media, *J. Acoust. Soc. Am.* 89 (4) (1991) 1521–1531.
- [31] M.J.S. Lowe, Matrix techniques for modeling ultrasonic waves in multilayered media, *IEEE Trans. Ultrason. Ferroelectr. Freq. Control.* 42 (4) (1995) 525–542.
- [32] S.I. Rokhlin, L. Wang, Ultrasonic waves in layered anisotropic media: characterization of multidirectional composites, *Int. J. Solids Struct.* 39 (2002) 5529–5545.
- [33] A. Velichko, P.D. Wilcox, Modelling the excitation of guided waves in generally anisotropic multi-layered media, *J. Acoust. Soc. Am.* 121 (2007) 60–69.
- [34] E. Glushkov, N. Glushkova, A. Eremin, Forced wave propagation and energy distribution in anisotropic laminate composites, *J. Acoust. Soc. Am.* 129 (5) (2011) 2923–2934.
- [35] E. Glushkov, N. Glushkova, S. Fomenko, Wave energy transfer in elastic half-spaces with soft interlayers, *J. Acoust. Soc. Am.* 137 (4) (2015) 1802–1812.
- [36] V. Giurgiutiu, Tuned lamb wave excitation and detection with piezoelectric wafer active sensors for structural health monitoring, *J. Intell. Mater. Syst. Struct.* 16 (4) (2005) 291–305.
- [37] E. Glushkov, et al., Evaluation of effective elastic properties of nitride NWs/polymer composite materials using laser-generated surface acoustic waves, *Appl. Sci.* 8 (2018) 2319.